Available online at www.sciencedirect.com
ScienceDirect
Journal of Power Sources 171 (2007) 966–980
JOURNAL OF POWER SOURCES
www.elsevier.com/locate/jpowsour

Review

Advances in Fe(VI) charge storage Part I. Primary alkaline super-iron batteries

Xingwen Yu [a,*], Stuart Licht [b]

[a] *Department of Chemical and Biological Engineering, The University of British Columbia, 2360 East Mall, Vancouver, BC, Canada V6T 1Z3*
[b] *Department of Chemistry, University of Massachusetts Boston, Boston, MA 02125, United States*

Received 27 May 2007; accepted 4 June 2007
Available online 26 June 2007

Abstract

Recent advances in super-iron batteries, based on an unusual Fe(VI) cathodic charge storage, are presented. Fe(VI) cathodes that have been demonstrated in super-iron batteries include the synthesized Fe(VI) compound with three-electron cathodic charge capacity Na_2FeO_4, K_2FeO_4, Rb_2FeO_4, Cs_2FeO_4 (alkali Fe(VI) salts), alkali earth Fe(VI) salts $BaFeO_4$, $SrFeO_4$, and also a transition Fe(VI) salt Ag_2FeO_4 which exhibits a five-electron cathodic charge storage. This paper focus on the primary alkaline Fe(VI) charge storage in aqueous electrolyte systems. Primary alkaline super-iron batteries exhibit a higher capacity than conventional alkaline batteries. Configuration optimization, enhancement and mediation of Fe(VI) cathode charge transfer of primary Fe(VI) alkaline batteries are summarized. Composite Fe(VI)/Mn(IV or VII), Fe(VI)/Ag(II) and zirconia coating stabilized Fe(VI)/Ag(II) cathode alkaline batteries are also illustrated.

Keywords: Fe(VI); Charge storage; Super-iron battery; Primary; Alkaline electrolyte

Contents

* Corresponding author. Tel.: +1 604 728 8895; fax: +1 604 822 6003.
E-mail address: xingwenyu@yahoo.com (X. Yu).

0378-7753/$ – see front matter © 2007 Elsevier B.V. All rights reserved.
doi:10.1016/j.jpowsour.2007.06.052

1. Introduction

Fe(VI) species have been known for over a century, although its chemistry remains relatively unexplored [1–3]. Fe(III) compounds had been explored both as cathode [4] and anode [5] materials in electrochemical storage cells, however, higher valent, greater charge capacity, iron salts had not been previously considered, and the fundamental solubility and stability constraints on higher valent iron chemistry were not well established. Indeed, the perception that Fe(VI) species were intrinsically unstable was incorrect [6]. Recently, cathodes incorporating hexavalent, Fe(VI), sustaining facile, energetic, cathodic charge transfer have been introduced [6–32]. Resources to prepare Fe(VI) salts are plentiful and clean. Iron is the second most abundant metal in the earth's core, and the Fe(VI) reduction product is non-toxic ferric oxide. Fe(VI) salts can exhibit substantially higher than conventional cathodic storage capacities [6–32]. Due to their highly oxidized iron basis, multiple electron transfer, and high intrinsic energy, it has been defined high oxidation state iron compounds as 'super-iron's and the new electrochemical storage cells containing them as 'super-iron' batteries [6].

Capacity, power, cost, and safety factors have led to the annual global use of approximately 6×10^{10} primary batteries, but further advances are limited by the low energy capacity of their cathodes. New higher capacity, environmentally benign and cost effect cathode materials are needed. International interest in Fe(VI) electrochemistry is growing, including research efforts in China, Canada, Europe, and Japan [33–36]. Favorable battery cathodes characteristics are low solubility, stability, facile charge transfer, and high charge capacity, and oxidative electrochemical potential. K_2FeO_4, prepared as described in Ref. [11], is particularly robust. So far, the controlled syntheses of a wide range of Fe(VI) salts have been probed [9,11–13,18,23,25], including a direct route for their electrochemical synthesis from iron metal [23].

This paper focuses on the recent advances in Fe(VI) charge storage in aqueous electrolyte systems and the primary alkaline super-iron batteries.

2. Fundamentals and charge storage advantages of primary alkaline super-iron batteries

In 1999, Licht's group introduced a class of batteries, referred to as super-iron batteries, containing a cathode utilizing a common material (iron) in an unusual (+6) valence state [6]. The cathode is based on abundant starting materials and is compatible with an alkaline electrolyte and zinc anode. Among the different types of aqueous primary batteries available on the market, the $Zn–MnO_2$ system possesses the dominant share for over a century because of its appropriate performance and low cost. The storage capacity of the aqueous MnO_2/Zn battery is limited by the charge capacity of MnO_2 (308 mAh g^{-1}), compared to that of Zn (820 mAh g^{-1}). Replacement of the MnO_2 cathodes in these cells with a more energetic cathode such as Fe(VI) compounds can substantially increase the energy storage capacity of these cells. For example, using the same zinc anode and electrolyte, Fe(VI) cathode batteries were shown to provide 50% more energy capacity than in conventional alkaline batteries [6].

2.1. Fundamentals of alkaline super-iron batteries

Using Fe(VI) compounds as charge storage materials is based on the three-electron reduction of Fe(VI) via Eq. (1) or Eq. (2) (as the anhydrous product), which represent energetic and high-capacity source of cathodic charge [6]:

$$FeO_4^{2-} + 3H_2O + 3e^- \rightarrow FeOOH + 5OH^- \quad (1)$$

$$FeO_4^{2-} + (5/2)H_2O + 3e^- \rightarrow (1/2)Fe_2O_3 + 5OH^-,$$
$$E = 0.5\text{–}0.65\ \text{V versus SHE} \quad (2)$$

So far, a class of Fe(VI) salts are successfully synthesized, include the alkali Fe(VI) salts (high purity K_2FeO_4, Cs_2FeO_4, Rb_2FeO_4 and $K_xNa_{(2-x)}FeO_4$, low purity Li_2FeO_4), high purity alkali earth Fe(VI) salts ($BaFeO_4$ and $SrFeO_4$) and a transition metal Fe(VI) salt (Ag_2FeO_4). Theoretical three-electron charge capacity of the Fe(VI) salts are determined as: 3 F MW^{-1}, from the salt molecular weight, MW(g mol^{-1}) and the Faraday constant (F = 96,485 coulomb mol^{-1} = 26,801 mAh mol^{-1}). Theoretical capacities of various alkali and alkali earth Fe(VI) salts are listed in Table 1.

Ag_2FeO_4 is of interest, as this Fe(VI) salt commands an intrinsic cathodic capacity that includes not only the three-electron Fe(VI) reduction, but also the single electron reduction of each of two Ag(I) (as shown in Eq. (3)), for at total 5 Faraday

Table 1
Theoretical three-electron charge capacities of various Fe(VI) salts

Fe(VI) salts	Theoretical capacity (mAh g^{-1})
Li_2FeO_4	601
Na_2FeO_4	485
K_2FeO_4	406
Rb_2FeO_4	276
Cs_2FeO_4	209
$SrFeO_4$	388
$BaFeO_4$	313

per mole or 399.3 mAh g^{-1} intrinsic capacity [26]:

$$Ag_2FeO_4 + (5/2)H_2O + 5e^- \rightarrow 2Ag + (1/2)Fe_2O_3 + 5OH^- \quad (3)$$

Primary alkaline super-iron battery was prepared with the same Zinc anode and alkaline electrolyte as the conventional alkaline batteries. In a zinc alkaline battery, the zinc anode generates a distribution of zinc oxide and zincate products, while similarly the final Fe(VI) product will depend on the depth of discharge. The general discharge of alkaline electrolyte cells utilizing a Zn anode and Fe(VI) cathodes is expressed as

$$MFeO_4 + (3/2)Zn \rightarrow (1/2)Fe_2O_3 + (1/2)ZnO + MZnO_2,$$
$$M = Li_2, Na_2, K_2, Ru_2, Cs_2, Sr, Ba \quad (4)$$

According to Eq. (3), the discharge of alkaline Ag_2FeO_4 cathode, Zn anode super-iron cell, will be expressed as

$$Ag_2FeO_4 + (5/2)Zn \rightarrow (1/2)Fe_2O_3 + 2Ag + (5/2)ZnO \quad (5)$$

The alkaline super-iron batteries were probed in either a 'coin cell' or an 'AAA cell' configuration. The cathode composite was formed by mixing a specified mass of Fe(VI) salt with an indicated weight percent of various carbon (carbon black or graphite) as the conductive matrix or other additives. Super-iron coin cells with a zinc anode were prepared from a conventional 1.1 cm diameter 'button' battery cell. The cells were opened, the anode and separator retained, and the cathode replaced with the new Fe(VI) cathode in the cell. In super-iron AAA experiments, components were removed from standard commercial alkaline cells (a cylindrical cell configuration with diameter 10.1 mm, and a 42 mm cathode current collector case height), and the outer MnO_2 mix replaced with a pressed Fe(VI) mix, followed by inclusion of the separator, Zn anode mix, gasket, and anode collector and resealing of the cell. Cells were discharged with a constant current, constant load or constant power function. Cell potential variation over time was measured via LabView Data Acquisition on a PC, and cumulative discharge, as ampere hours or as watt hours, determined by subsequent integration. The theoretical charge capacity is calculated by the (3 F mol^{-1}, F = Faraday, converted to ampere hours) measured cathode mass of the Fe(VI) salt. The three-electron Fe(VI) faradaic efficiency is determined by comparison of the measured cumulative ampere hours of discharge to the theoretical charge capacity [6–10].

2.2. Charge storage advantages of alkaline super-iron batteries: comparison with conventional MnO_2/Zn alkaline battery

High purity K_2FeO_4 and $BaFeO_4$ are readily synthesized through chemical methodology, with synthesis details described in reference [11]. Coupled with the Zn anode, generally, the open-circuit potential of $BaFeO_4$ super-iron battery is 1.85 V, 0.1 V higher than that of K_2FeO_4 battery at 1.75 V [6]. On the basis of open-circuit potential and Eq. (2), the K_2FeO_4/Zn and $BaFeO_4$/Zn batteries possess a respective maximum energy capacity of 475 Wh kg^{-1} and 419 Wh kg^{-1}, both higher than the maximum of 323 Wh kg^{-1} for a MnO_2/Zn battery.

The energy capacities of K_2FeO_4, $BaFeO_4$ and conventional MnO_2 cathode, alkaline primary batteries with a Zn anode were compared in Fig. 1a.

In both the low- (6000 Ω, current density $J = 0.25$ mA cm^{-2}) and high- (500 Ω, $J = 3$ mA cm^{-2}) discharge domain, the K_2FeO_4 cell generates a significantly higher capacity than does the MnO_2 cell. Of the three cells examined, the $BaFeO_4$ cathode cell exhibits the highest coulombic efficiency at high discharge rates ($J > 10$ mA cm^{-2}), resulting in the observed higher energy capacity despite the lower intrinsic charge capacity of $BaFeO_4$ compared to K_2FeO_4. The benefit of the facile charge-transfer capabilities of the conductive $BaFeO_4$ salt is evident in a cylindrical cell configuration (Fig. 1b). Discharge to 1 V at 0.7 W high constant power, the $BaFeO_4$ cell provides 200% higher energy compared to the advanced MnO_2 alkaline cylindrical cell [6].

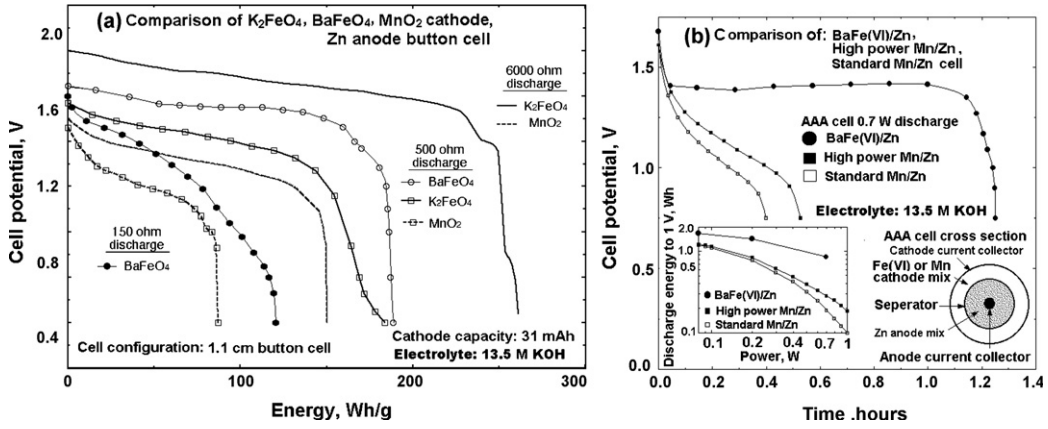

Fig. 1. (a) Energy capacity of K_2FeO_4, $BaFeO_4$ and conventional MnO_2 cathode alkaline primary batteries with a Zn anode. (b) The discharge of $BaFeO_4$ compared to standard or high-power alkaline MnO_2 in AAA cylindrical cell configuration. Main portion: cell potential measured during constant power discharge. Inset: measured energy capacity (Wh) vs. power (W) for the $BaFeO_4$, high-power, or standard alkaline MnO_2 cells [6].

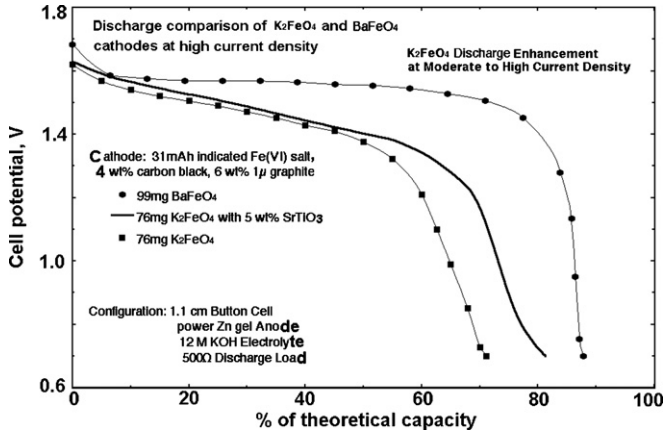

Fig. 2. The improved faradaic efficiency of a K_2FeO_4 cathode cell with a titanate additive. The percent of theoretical capacity is determined by the measured cumulative ampere hours, compared to the calculated ampere hours in the 3 F mol^{-1} measured mass of the Fe(VI) salt [10].

3. Optimization and charge transfer enhancement of K_2FeO_4, $BaFeO_4$ alkaline super-iron batteries

3.1. Discharge efficiency of K_2FeO_4, $BaFeO_4$ alkaline super-iron batteries and $SrTiO_3$, $Ba(OH)_2$ additives

At high load (current densities above 1 mA cm^{-2}) the faradaic efficiency of Fe(VI) reduction is significantly higher for a $BaFeO_4$ cathode compared to a K_2FeO_4 cathode, as shown in Fig. 2. In KOH electrolytes, titanates (Ti(IV) salts) have been utilized to improve the high current density utilization of the one-electron reduction of MnO_2 [37]. The similar phenomenon was also observed for the K_2FeO_4 faradaic efficiency. The improvement in K_2FeO_4 charge transfer was observed for a $SrTiO_3$ additive, which as presented in Fig. 2 under the indicated 500 Ω discharge load (equivalent to a current density of ∼3 mA cm^{-2}), improves the three-electron utilization from ∼68 to 77% (as measured by the fraction of the available 31 mAh discharged to a 0.8 V cutoff).

The fundamental solubility and stability of K_2FeO_4 and $BaFeO_4$ in alkaline electrolyte have been probed [7]. K_2FeO_4 solubility may be controlled over several orders of magnitude through the judicious choice of an alkali solution, while a very low (sub millimolar) K_2FeO_4 solubility can be achieved in a KOH electrolyte also containing $Ba(OH)_2$. In highly concentrated hydroxide, both KOH and CsOH electrolytes suppress K_2FeO_4 solubility. Solubility of K_2FeO_4 and $BaFeO_4$ in various alkaline electrolytes (various concentrations and various cation hydroxides) has been studied in detail in Ref. [7]. In the K_2FeO_4 case the higher KOH concentration the lower of the solubility of K_2FeO_4. $BaFeO_4$ is insoluble in water and has a solubility less than 2×10^{-4} M in 5 M KOH containing $Ba(OH)_2$. The resultant very low Fe(VI) solubility is advantageous, diminishing the possibility for self discharge in the super-iron battery [7]. For a fresh prepared cell, the discharge behavior has no difference when the KOH electrolyte is over 6 M. In this paper, the cells were prepared and studied in different years with different concentrations of KOH solution and are indicated in each figure. Electrolyte choices for alkaline batteries is based on the low solubility of Fe(VI) salts. Similarly, small amounts of $Ba(OH)_2$ added to the Fe(VI) cathode can constructively enhance the Fe(VI) insolubility in the alkaline electrolyte. To a K_2FeO_4 cathode, added $Ba(OH)_2$ can enhance charge transfer of the battery due to the partial conversion of K_2FeO_4 to $BaFeO_4$ in the alkaline electrolyte [7,10]:

$$K_2FeO_4 + Ba(OH)_2 \rightarrow BaFeO_4 + 2KOH \quad (6)$$

3.2. Mn(IV), Co(III) modifiers and their effects on super-iron batteries

The Fe(VI) battery potential can be shifted and controlled by specific modifiers. Small modifications (in the order of a 0.1–10% by weight) of the Fe(VI) cathode can be used to either substantially enhance or diminish the discharge potential. Specifically, as shown in Fig. 3a, the average discharge potential of the $BaFeO_4$ cell is increased by an average of ∼150 mV when a relatively small percent of Co_2O_3, is mixed with the $BaFeO_4$. Alternately, the average discharge potential is decreased by an average of ∼200 mV when 1% of MnO_2 is used to modify the $BaFeO_4$.

Interestingly, these modifiers do not significantly affect the open circuit cathode potential of 1.84–1.89 V measured versus the Zn anode nor do these modifications significantly affect the high faradaic efficiency of the three-electron reduction [8]. Such effects are useful to provide control of the super-iron battery dis-

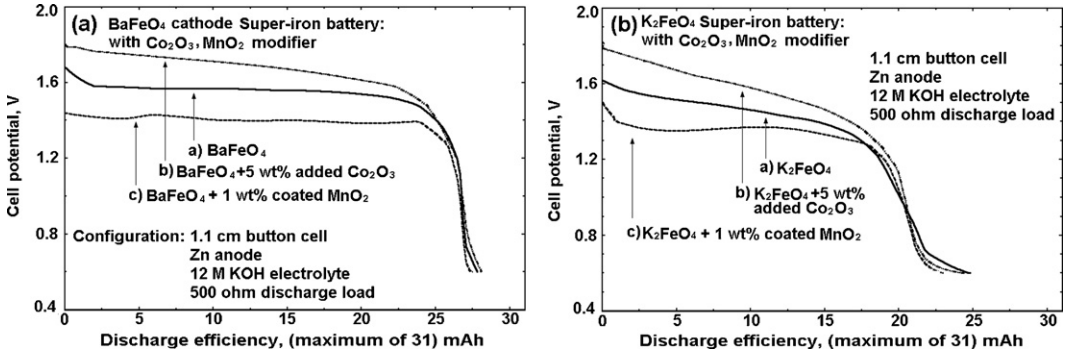

Fig. 3. Super-iron (Zn anode) batteries treated with solid phase cathode modifiers, added Co_2O_3 or coated MnO_2: (a) $BaFeO_4$-Zn cell; (b) K_2FeO_4-Zn cell. The cathode mix also contains 10% carbon by mass [8].

charge potential. These effects are also generalized to K_2FeO_4 cathodes (Fig. 3b).

Chemical mediation of Fe(VI) charge transfer with permanganate and manganate will be presented in Section 3. Here, the advantage of Fe(VI) remediation with Mn(VII), Mn(VI) was taken to coat the Fe(VI) particles with a small overlayer of MnO_2, which can have a dramatic effect on the discharge potential of the super-iron battery [8]. The coating procedure is detailed in reference [8]. Normally, if K_2FeO_4 powder is coated with an excess of manganate or permanganate, the cell potential is not significantly affected. However, when the K_2FeO_4 powder is coated to a low level, as seen in Fig. 3b with the 1% $KMnO_4$-coated K_2FeO_4 powder, the cell exhibits a discharge potential diminished by 150 mV.

The following proposed model [8] appears to be consistent with the observed decrease in potential of this Mn-coated super-iron: the decreased Fe(VI) potential is due to the intermediate reduction of Mn(IV) surface states which are electrocatalytically active in accord with the following equation:

$$3MnO_2 + (3/2)H_2O + 3e^- \rightarrow (3/2)Mn_2O_3 + 3OH^-, \quad E = 0.3\ \text{V versus SHE} \tag{7}$$

Following reduction, discharged manganese sites are reactivated by the remaining Fe(VI) in the chemical step:

$$(3/2)Mn_2O_3 + FeO_4^{2-} + H_2O \rightarrow 3MnO_2 + (1/2)Fe_2O_3 + 2OH^- \tag{8}$$

The renewed MnO_2 can then continue to catalyze the Fe(VI) reduction, in accord with the electrochemical and chemical steps summarized by a repetitions of Eqs. (7) and (8). In accord with this mechanism, Fe(VI) reduction will occur at a potential shifted towards the MnO_2 reduction potential, nevertheless accessing the intrinsic faradaic capacity of the Fe(VI) cathode [8].

An understanding of the observed Co(III) effect of a significant potential increase shown in Fig. 3 is facilitated by a review of Co alkaline electrochemistry [8]. Of significance is the emphasis by Gohr [38] of a Co(IV) oxide which may be reduced in alkaline solutions at a potential which is 0.1–0.2 V higher than the Fe(VI) potential, and therefore is consistent with the observed increase in the Fe(VI) cathode discharge potential:

$$CoO_2 + 2H_2O + e^- \rightarrow Co(OH)_3 + OH^-, \quad E = 0.7\ \text{V versus SHE} \tag{9}$$

which indicates that the Fe(VI) potential is insufficient for Co(III) oxidation to Co(IV). Nevertheless the potentials are close, and one hypothesis is that a Nernst shift of potentials, sufficient for Fe(VI) to oxidize Co(III), may occur for example in an excess of Fe(VI), and at the electrode | concentrated hydroxide interface. This hypothesis suggests a mechanism for the observed Co(III) enhancement of the super-iron potential via an electrochemically active Co(IV) intermediate state:

$$3Co(OH)_3 + FeO_4^{2-} \rightarrow 3CoO_2 + (1/2)Fe_2O_3 + (7/2)H_2O + 2OH^- \tag{10}$$

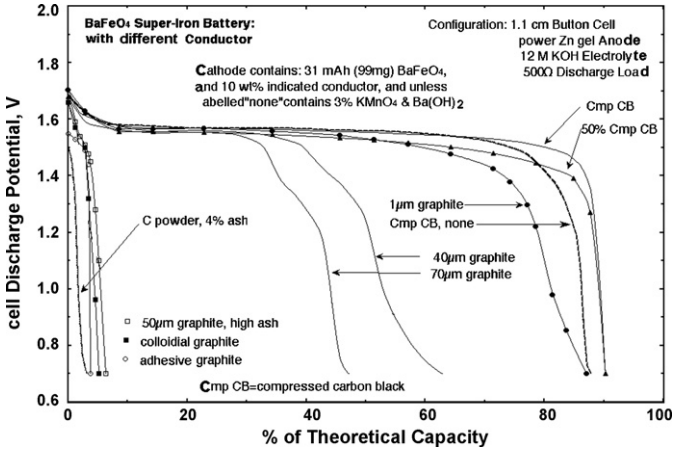

Fig. 4. The effect of carbon based cathode conductive additive on the discharge of super-iron ($BaFeO_4$-Zn) batteries [10].

The electrochemical discharge of the Co(IV) intermediate follows Eq. (9) and thereby releases Co(III) for continued catalysis of the Fe(VI) reduction in accord with Eqs. (9) and (10) [8].

3.3. Various carbon conductors and their effects on super-iron batteries

One micron graphite and carbon black are the two best conductive matrix to support Fe(VI) cathodes discharge. Various carbon materials were probed, added as a conductive matrix to support Fe(VI) reduction. However, as seen in Fig. 4, most of them yield a low Fe(VI) discharge capacity. These observed low discharge capacities may be due to several factors including (i) high intrinsic resistance of the added 'conductor', (ii) poor electron transfer between the clean conductor | Fe(VI) interface, and (iii) reaction and passivation of the conductor | Fe(VI) interface [10].

The carbon based materials added to the Fe(VI) cathode are observed to be described by three categories in Fig. 4, which consist of materials supporting either efficient, intermediate, or inefficient Fe(VI) charge transfer. The inefficient category includes carbon powder with 4% ash, high ash, colloidal, and adhesive graphites. The intermediate category includes the 40 and 70 μm particle size graphites. Finally, the efficient Fe(VI) charge transfer category comprises carbon black (either 50% or fully compressed) and 1 μm graphite. As seen in the figure, the fully compressed carbon black provides improved super-iron battery discharge characteristics compared to the 50% compressed carbon black cathode conductor. As also noted in the figure, a small (3%) addition to the cathode of $KMnO_4$ and $Ba(OH)_2$ can further improve the discharge characteristics [10].

3.4. Fluorinated polymer graphite conductor and its effects on super-iron batteries

Fluorinated polymer graphite has an interesting effect on the discharge of super-iron battery [10,15], as presented in Fig. 5.

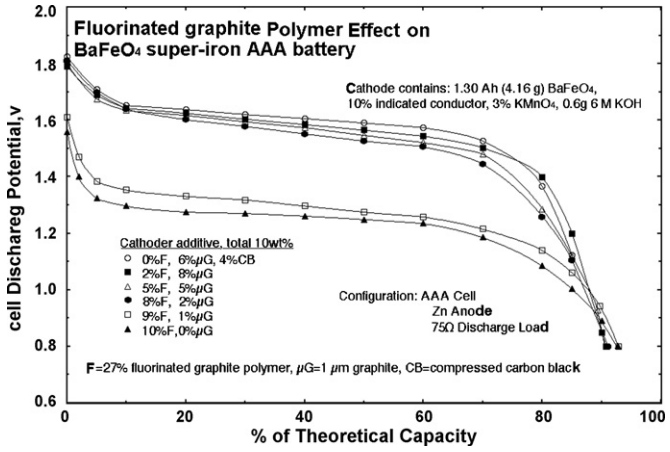

Fig. 5. The effect of fluorinated graphite polymer as a cathode additive on the discharge of $BaFeO_4$-Zn AAA cylindrical batteries [10].

As seen in the top curve of Fig. 5, and consistent with the results of Fig. 2, a mix of 1 μm graphite and carbon black sustains a high discharge potential throughout an efficient three-electron reduction of the Fe(VI). The fluorinated polymer graphite can be used to effectively control the cell discharge potential while maintaining a high discharge efficiency. The lowest curve in Fig. 5 was obtained with a Fe(VI) cathode mix containing only the 27% fluorinated polymer graphite (FG(27%)). A lower, but significant discharge voltage of 1.2–1.3 V is sustained. Despite these significant polarization losses, this conductor supports a somewhat higher Fe(VI) faradaic efficiency than that observed with the graphite/carbon black conductor. As seen in the figure, replacement of 1% of the FG(27%) with the 1 μm graphite has little effect on the discharge potential. The observed faradaic efficiency of approximately 92% is yet higher. Replacement of higher amounts of the FG(27%) with the 1 μm graphite provides control of the discharge voltage. The discharge voltage jumps by 300 mV when 2% of 1 μm graphite is utilized and as seen in the figure, the discharge potential continues to increase when 5% of 1 μm graphite is utilized. Finally, as seen comparing the top two curves of the figure, the Fe(VI) mix, containing 2% FG(27%) and 8% 1 μm graphite, provides a marginally higher faradaic efficiency, albeit at marginally lower discharge potential, compared to the cathode mix containing 1 μm graphite and carbon black cathode.

Further presented in Fig. 6a, a cell with a 10 wt% of FG(27%) conductor, does not exhibit an evident greater storage capacity than the graphite/carbon black cell. However, cells using 10 wt% of FG(58%), not only exhibit a higher storage capacity, but as seen in the figure, this nominal storage capacity is over 100% of the theoretical capacity of $BaFeO_4$. This effect was further explored with the additional set of cathode mixes containing a higher weight fraction of the added conductor, as shown in Fig. 6b.

As shown in Fig. 2, at high load, the faradaic efficiency of K_2FeO_4 cathode is low. But at lower current densities and high fraction of graphite, K_2FeO_4 is also expected to approach discharging to the theoretical $3e^-$/Fe(VI). As seen in Fig. 6b, the discharge of 10 wt% K_2FeO_4 in 90 wt% 1 μm graphite, leads to the expected near 100% of the theoretical $3e^-$ storage capacity (406 mAh g^{-1} K_2FeO_4). Unexpectedly, replacement of this high fraction of graphite with an equal mass (90 wt%) of FG(27%), leads to nearly 200% of the theoretical storage capacity. Combining with $KMnO_4$, a cell containing both 5 wt% K_2FeO_4 and 5 wt% $KMnO_4$ with 90 wt% of this FG exhibits over 175% of the theoretical three-electron storage capacity. By comparison, a cell containing both 5 wt% $BaFeO_4$ and 5 wt% $KMnO_4$ with 90 wt% of this FG(27%) exhibits nearly 200% of the theoretical three-electron storage capacity [15].

The unusual effects of FG conductors on the discharge of super-iron batteries are related to the intrinsic alkaline cathode capacity in FGs which does not occur in conventional graphites or carbon blacks [15]. The FG polymers are observed to simultaneously maintain two roles in the cathode composite; functioning both as a conductive matrix, and also adding intrinsic capacity to the cathodes [15].

4. Chemical mediation of Fe(VI) charge transfer and Fe(VI)/Mn composite super-iron batteries

4.1. Inhibition of Fe(VI) charge transfer

The alkaline galvanostatic reduction of solution phase Fe(VI) on Pt generates an observable solid Fe(III) overlayer and sus-

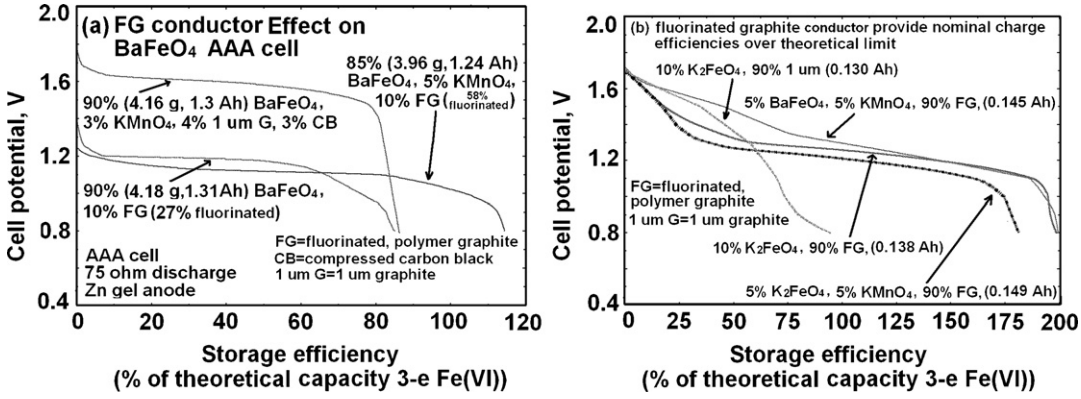

Fig. 6. Discharge comparison using (a) low weight; (b) high weight fractions of conventional or FG conductors in the cathode composite of super-iron K_2FeO_4, $BaFeO_4$ AAA batteries. Anode of the cell is Zn, and 13.5 M KOH was used as electrolyte [15].

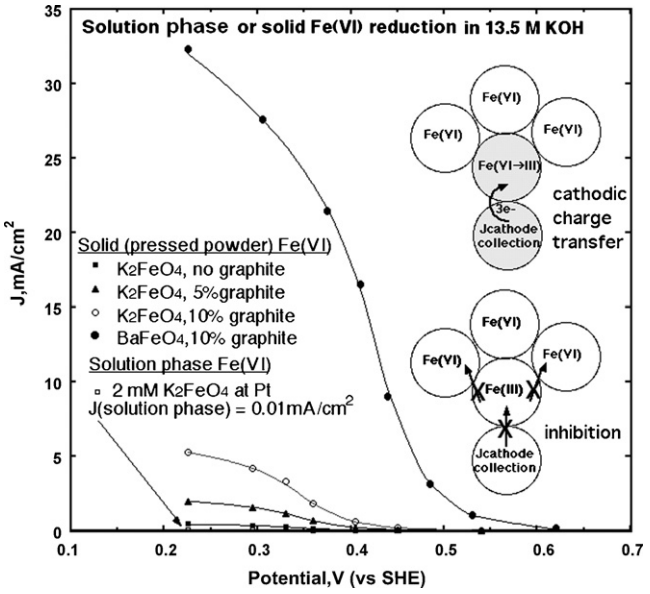

Fig. 7. Galvanostatic reduction on Pt for 2 mM K_2FeO_4 in 13.5 M KOH or the indicated pressed Fe(VI) powders on Pt in 13.5 M KOH [20].

tains cathodic current densities of only less than 100 μA cm^{-2}. As seen in the comparison in Fig. 7, solid Fe(VI) cathodes can sustain two orders of magnitude higher current density, which is highest when mixed with several percent of graphite.

As represented in the scheme included within the figure, Fe(VI) charge transfer inhibition, when occurring, appears directly related to buildup of a low conductivity Fe(III) reduction product at the Fe(VI)/cathode current collector interface. The Fe(III) products have been studied with FTIR, ICP, and X-ray powder diffraction [12]. From the FTIR, these Fe(VI) discharge products contain hydroxide and Fe(III) salts, but the amorphous nature of the observed spectra does not lead to identification of the specific $M_aFe(III)O_x(OH)_y(H_2O)_z$ product (M = K_2 or Ba). It is reasonable to assume that the product will vary with pH, the extent of hydration, and the degree of Fe(VI) discharge. Thus, the coexisting product stoichiometries may include:

$$Fe_2O_3 + xH_2O \Leftrightarrow 2FeOOH\cdot(x-1)/2H_2O \quad (11)$$

$$Fe_2O_3 + xBa(OH)_2 \Leftrightarrow Ba_xFe_2O_{(3+x)}\cdot yH_2O + (x-y)H_2O \quad (12)$$

$$Fe_2O_3 + 2xKOH \Leftrightarrow K_{2x}Fe_2O_{(3+x)}\cdot yH_2O + (x-y)H_2O \quad (13)$$

It is evident from the observed higher relative coulombic efficiencies of $BaFeO_4$ cathodes, and from the high current densities sustained in Fig. 7, that the barium product of a $BaFeO_4$ reduction does not inhibit charge transfer to the degree of inhibition of the potassium product of K_2FeO_4 reduction. This is consistent with the results shown in Fig. 2.

4.2. Chemical mediation of Fe(VI) charge transfer

Licht's group have probed the Mn(VI), Mn(VII) improvement of (both potassium and barium) Fe(VI) charge transfer [8,14]. A mechanism consistent with this facile charge transfer is proposed as Fig. 8. With a similar alkaline potential, an analogous description for a manganate, Mn(VI), facilitated Fe(VI) process will be evident from Eq. (15), but is not included in Fig. 8 description for clarity. The process utilizes the overlapping energetics of Mn(VII) and Fe(VI) redox chemistry to provide alternate pathways to minimize the effect summarized in Fig. 7 of Fe(III) charged transfer inhibition and promoting Fe(VI) regeneration. The driving force for the Fe(VI) regeneration is the chemical and potential gradient that will spontaneously arise as the cathode discharges which as described in Fig. 8 creates an anodic shift in more highly reduced portions of the cathode. Fe(III) at these sites is spontaneously regenerated to nonpassivating Fe(VI) by Mn(VII), as expressed by

$$2MnO_4^- + Fe_2O_3 + 2OH^- \leftrightarrow 2MnO_2 + 2FeO_4^{2-} + H_2O \quad (14)$$

(or via manganate as expressed by)

$$3MnO_4^{2-} + H_2O + Fe_2O_3 \leftrightarrow 3MnO_2 + 2OH^- + 2FeO_4^{2-} \quad (15)$$

This same potential gradient will drive Mn(IV) regeneration to Mn(VII) via interior (bulk) Fe(VI) and the reverse reaction described in Eq. (14). This provides a charge shuttle to access bulk Fe(VI), which is only possible due to the near lying redox potentials of the Fe(VI/III) and Mn(VII/IV) half reactions. As detailed in Fig. 8, the process may be summarized by the cocathode chemical mediation of the Fe(VI/III) redox reaction to prevent Fe(VI) depletion near the cathode current collector and provide facile charge-transfer according to

$$Fe(VI)_{collector} + 3e^- \rightarrow Fe(III)_{collector} \quad (16)$$

$$Fe(III)_{collector} + Mn(VII) \rightarrow Fe(VI)_{collector} + Mn(IV) \quad (17)$$

$$Fe(VI)_{bulk} + Mn(IV) \rightarrow Fe(III)_{bulk} + Mn(VII) \quad (18)$$

4.3. K_2FeO_4/Mn(VII or VI) composite super-iron batteries

The synergistic improvement of a K_2FeO_4 cathode with either $KMnO_4$ or $BaMnO_4$ is presented in the top 2 section of Fig. 9 and further detailed in Table 2.

As seen in Table 2, in addition to $KMnO_4$ and $BaMnO_4$, the K_2FeO_4 cathode can also be improved by inclusion of other activators individually or together with Mn(VII or VI). As detailed in the table, added salts, such as LiOH or NaOH do not increase a K_2FeO_4 cathode discharge. Also included in the table are relatively small, but significant, improvements of the K_2FeO_4 discharge energy with 10% addition of CsOH and $Ba(OH)_2$.

A composite K_2FeO_4/$BaMnO_4$ cathode yields a significantly higher energy capacity than a pure K_2FeO_4 cathode. As indicated in the top section of Fig. 9 as the open or solid small circles, added barium manganate can significantly enhance the

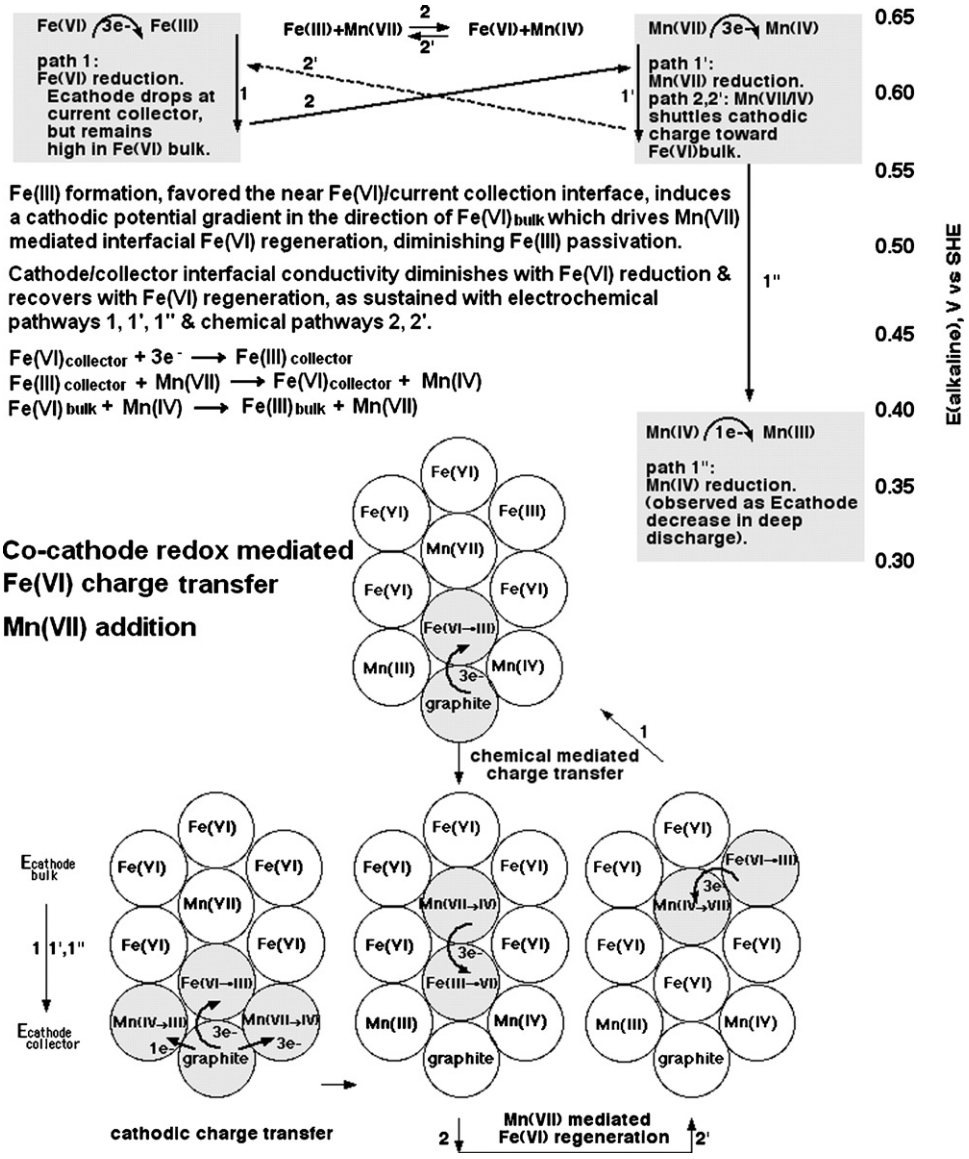

Fig. 8. Co-cathode redox mediated Fe(VI) charge transfer, exemplified by Mn(VII) addition. Composites with near lying redox processes provide multiple pathways to facilitate Fe(VI) charge transfer; illustrated here by energy, mechanism, and chemical schematic representation [20].

discharge energy of the K_2FeO_4 cathode. This is a synergistic effect, increasing the energy of either pure cathode alone. For the K_2FeO_4/$BaMnO_4$ composites, a maximum 2.8 Ω discharge energy of 0.78 Wh is measured for the cell containing 45 wt% K_2FeO_4 and 55 wt% $BaMnO_4$, which is more than double that seen for the pure K_2FeO_4 cathode. As detailed in Table 2 at the low rate (constant 75 Ω load), the K_2FeO_4/$BaMnO_4$ composite cathode exhibits a nearly constant maximum energy capacity of 1.2 Wh over a wide composition range varying from 33:67% to 67:33%. KOH or Al_2O_3 impairs the discharge effectiveness of the $BaMnO_4$/K_2FeO_4 composite cathode. But $Ba(OH)_2$ modestly increases the discharge energy of the composite $BaMnO_4$/K_2FeO_4 cathode due to the improvements of $Ba(OH)_2$ on the pure K_2FeO_4 electrode [20].

The discharge of K_2FeO_4/$KMnO_4$ composite cathodes was optimized with various additives. The $Ba(OH)_2$ was consistently the most effective additive with the high rate discharge summarized in the midsection of Fig. 9. In the presence of both Mn(VII) salts and Fe(VI), competing alkali earth hydroxide effects are complex. For example, in the reaction with $Ba(OH)_2$, the $KMnO_4$ reaction product $Ba(MnO_4)_2$ is highly soluble. However, the alternative reaction K_2FeO_4 with $Ba(OH)_2$ forms $BaFeO_4$, which is insoluble in water. As seen in the midsection portion of Fig. 9, the addition of $Ba(OH)_2$ to the K_2FeO_4/$KMnO_4$ cathode results in a significant increase in discharge energy, and at an average discharge potential greater than that observed for the K_2FeO_4/$KMnO_4$ composite without $Ba(OH)_2$. At both high and low rate, a maximum discharge energy is observed with the 33:57:10 wt% K_2FeO_4:$KMnO_4$:$Ba(OH)_2$ composition which provides 0.73 and 1.62 Wh, respectively over either 2.8 or 75 Ω load discharges [20].

$AgMnO_4$ provides an unusual salt in that the Ag valence acts in a manner intermediate to Ag(I) and Ag(II), that is as

Table 2
Comparison of the discharge behavior in alkaline AAA cell of a cathode composite containing K_2FeO_4/$BaMnO_4$ or K_2FeO_4/$KMnO_4$ (dry cathode composition, by mass discharge to 0.8 V, at constant load)

Fe salt	wt%	Mn salt	wt%	Salt	wt%	2.8 Ω		75 Ω	
						E (Wh)	V_{av} (V)	E (Wh)	V_{av} (V)
K_2FeO_4	100					0.28	1.17	0.68	1.36
K_2FeO_4	90			$Ba(OH)_2$	10	0.35	1.15	0.79	1.44
K_2FeO_4	90			LiOH	10	0.30	1.09	0.63	1.31
K_2FeO_4	90			NaOH	10	0.24	1.05	0.60	1.35
K_2FeO_4	90			CsOH	10	0.34	1.17	0.83	1.44
K_2FeO_4	0	$BaMnO_4$	100			0.37	1.16	0.96	1.19
K_2FeO_4	5	$BaMnO_4$	95			0.44	1.16	1.03	1.26
K_2FeO_4	10	$BaMnO_4$	90			0.54	1.17	1.14	1.31
K_2FeO_4	25	$BaMnO_4$	75			0.59	1.17	1.16	1.39
K_2FeO_4	33	$BaMnO_4$	67			0.65	1.19	1.20	1.40
K_2FeO_4	45	$BaMnO_4$	55			0.78	1.20	1.20	1.41
K_2FeO_4	50	$BaMnO_4$	50			0.67	1.20	1.20	1.41
K_2FeO_4	67	$BaMnO_4$	33			0.66	1.20	1.19	1.44
K_2FeO_4	75	$BaMnO_4$	25			0.57	1.22	1.12	1.45
K_2FeO_4	90	$BaMnO_4$	10			0.38	1.21	0.98	1.45
K_2FeO_4	95	$BaMnO_4$	5			0.38	1.19	0.71	1.43
K_2FeO_4	33	$BaMnO_4$	57	Al_2O_3	10	0.62	1.19	1.10	1.37
K_2FeO_4	57	$BaMnO_4$	33	Al_2O_3	10	0.56	1.17	1.13	1.43
K_2FeO_4	10	$BaMnO_4$	57	$Ba(OH)_2$	33	0.44	1.26	0.68	1.28
K_2FeO_4	33	$BaMnO_4$	34	$Ba(OH)_2$	33	0.60	1.28	0.92	1.51
K_2FeO_4	33	$BaMnO_4$	57	$Ba(OH)_2$	10	0.81	1.27	1.17	1.41
K_2FeO_4	50	$BaMnO_4$	25	$Ba(OH)_2$	25	0.78	1.28	1.15	1.51
K_2FeO_4	57	$BaMnO_4$	33	$Ba(OH)_2$	10	0.81	1.29	1.21	1.46
K_2FeO_4	57	$BaMnO_4$	10	$Ba(OH)_2$	33	0.76	1.29	1.27	1.61
K_2FeO_4	57	$KMnO_4$	10	$Ba(OH)_2$	33	0.63	1.26	1.04	1.16
K_2FeO_4	50	$KMnO_4$	50			0.47		1.41	

for $Ag(I+x)Mn(VII-x)O_4$, where $0<x<1$ [16,39]. Of the permanganate and manganate salts explored to date, $AgMnO_4$ promotes one of the larger increases in the K_2FeO_4 alkaline cathode discharge, a phenomenon consistent with the observed Ag activation of Fe(VI) (to be presented in the next section), but the $AgMnO_4$ activation phenomenon is only substantial in the presence of KOH (added as a solid salt to the mix) [16]. This is observed in the lowest section of Fig. 9. In the absence of KOH, the 2.8 Ω discharge of the K_2FeO_4 cathode increases from to 0.3 Wh to ~0.4 Wh with the addition of 18% $AgMnO_4$, but is enhanced to 0.5 Wh using only 12 wt% $AgMnO_4$ with KOH (6 wt%). This increase to ~0.8 Wh is with the inclusion of 38 wt% $AgMnO_4$ and 12 wt% KOH. Finally, as also seen in the figure, a K_2FeO_4, partially converted to the barium salt with a $Ba(OH)_2$ wash and mixed with $AgMnO_4$ and KOH, provides a cathode with a high rate discharge similar to the desired capacity of the $BaFeO_4$ cathode, exhibiting a higher energy capacity, but lower average discharge potential. Aspects of the intriguing KOH activation of the pure $AgMnO_4$ alkaline cathode (without K_2FeO_4) are explored in reference [16], and the $AgMnO_4$ activation of K_2FeO_4 is still lower than that observed for the AgO mediation of K_2FeO_4 charge transfer (see Section 5).

4.4. $BaFeO_4$/Mn(VII) composite super-iron batteries

The 75 Ω energy capacity of pure $BaFeO_4$ is 1.75 Wh with a discharge profile highly similar to that of the 95% $BaFeO_4$/5% $KMnO_4$ composite cathode (capacity of 1.8 Wh to a 0.8 V discharge) detailed in the top section of Fig. 10. As seen in the figure, cells containing high fractions of both $BaFeO_4$ and $KMnO_4$ discharge to a higher capacity. Hence, a cathode with either 50:50 or 75:25 relative weight percent of $BaFeO_4$ to $KMnO_4$ yields respective discharge capacities of 1.83 and 1.95 Wh. Utilization of a CsOH, rather than KOH electrolyte further enhanced the discharge energy to 2.1–2.2 Wh. The resultant volumetric capacity of 600 Wh cm^{-3} is high compared a maximum 400 Wh cm^{-3} for a high performance MnO_2 cathode alkaline AAA cell.

4.5. $BaFeO_4$/MnO_2 composite super-iron batteries

Due to the restriction use of barium salts by the US EPA [40], it is of interest to probe the MnO_2/$BaFeO_4$ composite cathodes with reduced barium levels. As seen in Fig. 11, due to the lower average voltage discharge for the pure MnO_2 cathode, its 0.7 W discharge is diminished compared to the 2.8 Ω. In comparison, high capacities are shown for both a constant load (2.8 Ω) discharge and for a constant power (0.7 W) discharge, for the cell containing a cathode composed primarily of $BaFeO_4$. As also presented in the figure, $BaFeO_4$/MnO_2 composites, containing less barium, exhibit significantly higher discharge energy compared to the MnO_2 cathode in conventional alkaline cells, and intermediate to the values observed for the MnO_2 free, $BaFeO_4$ cathode. Under the same 2.8 Ω load, high rate conditions, the 3:1 composite MnO_2/$BaFeO_4$ cathode cells yields 0.78 Wh to an 0.8 V discharge cut-off, providing ~30% additional capacity

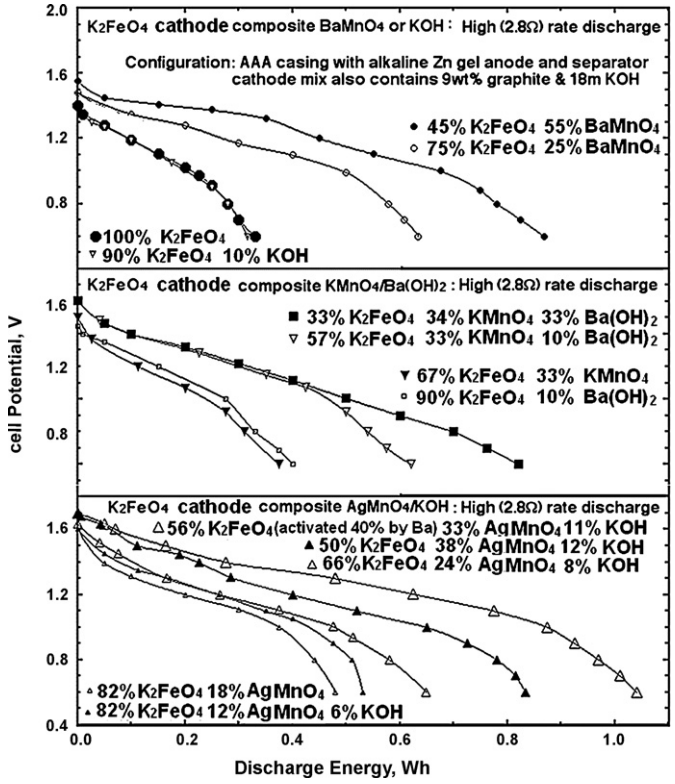

Fig. 9. Cell potential and energy capacity of alkaline cells with K_2FeO_4 composite cathodes containing various relative amounts of $BaMnO_4$, $KMnO_4$, $AgMnO_4$, $Ba(OH)_2$, or KOH, compared to K_2FeO_4 in the cathode mix, during discharge at a high constant load rate of 2.8 Ω. In the composite cells, the combined mass of the K_2FeO_4 and other salts is intermediate to the mass of the pure salts (a pure cathode contains 3.5 g K_2FeO_4, 4.2 g $BaFeO_4$, 4.1 g $BaMnO_4$, 3.5 g $KMnO_4$, or 4.6 g $AgMnO_4$). Cells use an alkaline AAA configuration including 9 wt% graphite and 18 M KOH electrolyte [20].

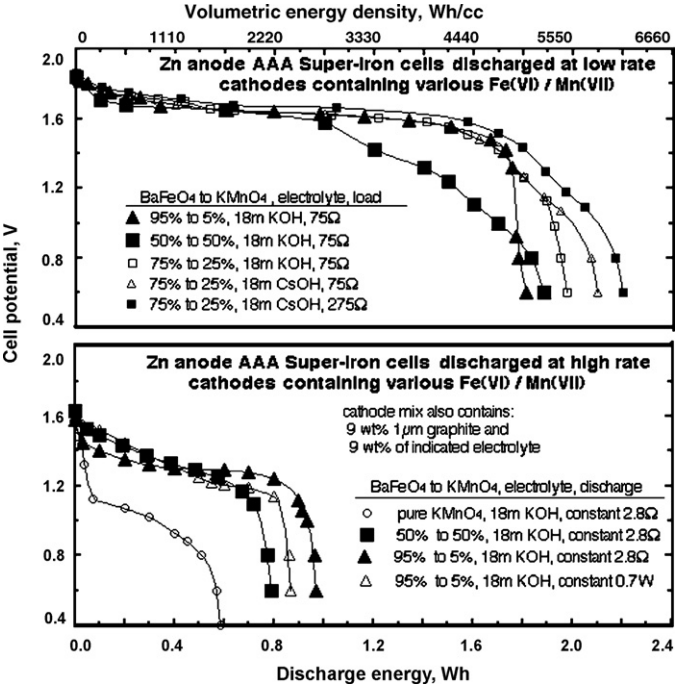

Fig. 10. Cell potential and energy capacity of alkaline super-iron AAA cells. Cells contain various indicated weight fractions of Fe(VI), Mn(VII), and Mn(VI) salts, in the cathode mix, and use either a KOH or CsOH electrolyte [14].

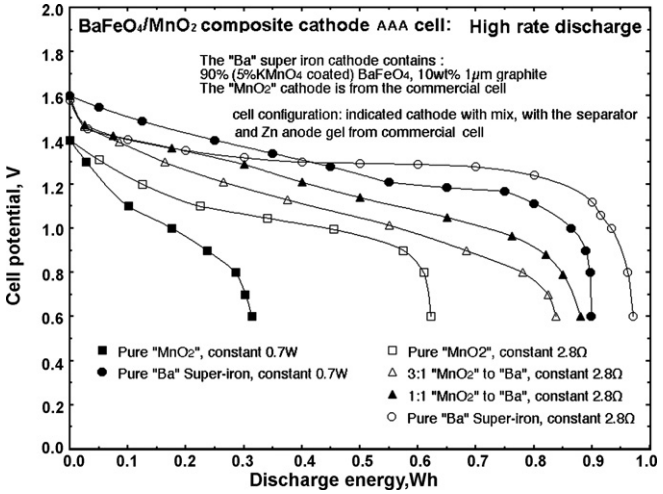

Fig. 11. The high power domain discharge of super-iron ($BaFeO_4$ and $BaFeO_4/MnO_2$ composites) compared to the discharge of MnO_2 cathode cells, each in a cylindrical (AAA) cell configuration [19].

compared to the 2.8 Ω pure MnO_2 cell discharge, and more than double the capacity of the pure MnO_2 0.7 W discharge. The 1:1 composite $MnO_2/BaFeO_4$ cathode cells yield 0.85 Wh to an 0.8 V discharge cut-off, providing ∼40% additional capacity compared to the 2.8 Ω pure MnO_2 cell discharge, and triple the capacity of the pure MnO_2 0.7 W discharge. *Note*: a 3:1 "MnO_2" to "Ba" composite cathode was prepared with 75% by mass of the dry MnO_2 cathode mix and 25% of the dry $BaFeO_4$ cathode mix, for a total dry mass of 4.9 g; a 1:1 "MnO_2" to "Ba" composite cathode was prepared with 50% by mass of the dry MnO_2 cathode mix and 50% of the dry $BaFeO_4$ cathode mix, for a total dry mass of 4.8 g. A 0.4 g of saturated KOH is added to each of the various cathode mixes [19].

5. Silver mediation of Fe(VI) charge transfer & zirconia coating stabilized Fe(VI)/AgO composite super-iron battery

5.1. Chemical and electronic mediation of Fe(VI) charge transfer

Fig. 12 is a model in a process for co-cathode electronic and redox mediated Fe(VI) charge transfer in which conductive composites with energetically near lying redox processes provide multiple pathways to facilitate Fe(VI) charge transfer [20].

In this figure, the process is exemplified by addition of an Ag(II) salt, in which the cathode/collector interfacial conductivity (a) increases with Ag(I) and Ag(0) formation, (b) diminishes with Fe(VI) reduction, and (c) recovers with Fe(VI) regeneration. An Ag(II) salt, such as AgO, as an Fe(VI) co-cathode is analogous to Mn(VII) and Mn(VI) in that it exhibits intrinsic two separate alkaline cathodic redox couples in the same potential domain as the single $3e^-$ Fe(VI) redox couple:

$$AgO + (1/2)H_2O + e^- \rightarrow (1/2)Ag_2O + OH^-,$$
$$E = 0.6\,\text{V versus SHE} \quad (19)$$

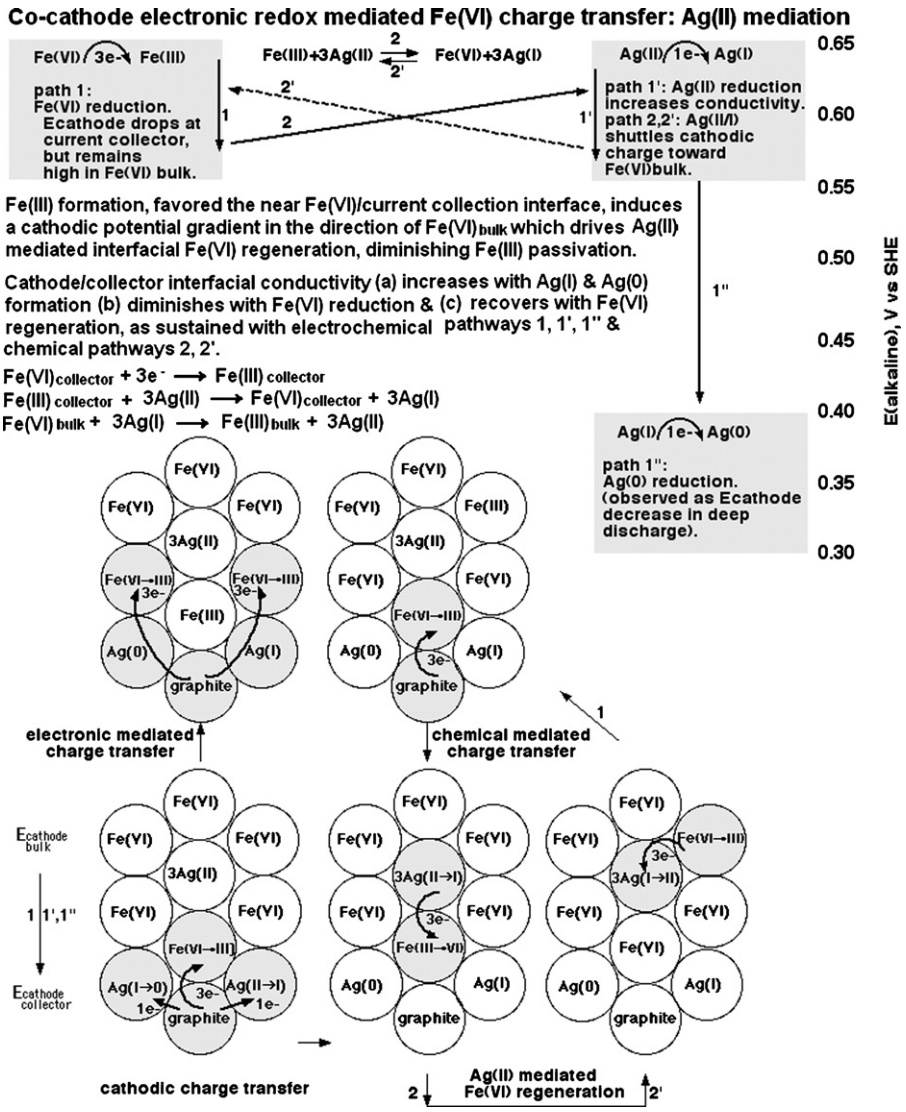

Fig. 12. Co-cathode electronic and redox mediated Fe(VI) charge transfer, exemplified by Ag(II) addition. Composites with near lying redox processes provide multiple pathways to facilitate Fe(VI) charge transfer; illustrated here by energy, mechanism, and chemical schematic representation [20].

$$(1/2)Ag_2O + (1/2)H_2O + e^- \rightarrow Ag + OH^-,$$
$$E = \sim 0.35\ \text{V versus SHE} \quad (20)$$

In comparison to the chemical mediation model of Fig. 8, in Fig. 12 the additional pathway for Fe(VI) charge transfer is evident in the mid-left chemical schematic labeled electronic mediated charge transfer. Concurrent with increasing cathode consumption is an increasing buildup of conductive Ag, providing electronic access to bulk Fe(VI). Silver is a superlative metallic conductor; as the AgO discharges, the concentration of reduced silver grows and provides a growing conductive matrix to increasingly facilitate the Fe(VI) reduction [20].

5.2. $MFeO_4$ (M = K_2 or Ba)/AgO composite cathode super-iron batteries

The activation of $BaFeO_4$ and K_2FeO_4 by AgO in Fig. 13 is substantial compared to that by $KMnO_4$ or $BaMnO_4$ observed in Figs. 9 and 10 and Table 2. As seen in Fig. 13b, as little as 7 wt% AgO composite with K_2FeO_4 yields a discharge energy comparable or larger than the 50 wt% of the $KMnO_4/K_2FeO_4$ composite cathode. At larger AgO fractions, high rate discharge energies as great as 1.5 Wh are observed. These discharge energies are substantially higher than conventional alkaline MnO_2 and are also higher than AgO (or $BaFeO_4$) alone.

The AgO has a synergistic activation on $BaFeO_4$ or K_2FeO_4 in which the combined discharge capacity of the composite Ag(II)/Fe(VI) cathode is larger than that of either cathode alone. As with K_2FeO_4, an unusually high energy discharge also occurs for an AgO cathode composite with the $BaFeO_4$ Fe(VI) salt. In Fig. 13a the $BaFeO_4$/AgO cathode mix maintains the unusual high-power characteristic known for the $BaFeO_4$ cathode without AgO. Hence, the $BaFeO_4$ cathode both with and without AgO generates a power of at least 0.7 W over a constant 2.8 Ω load. However, in addition, the Fe(VI) composite cathode unexpectedly discharges for ~170 min and generates 1.5 Wh, whereas under the same conditions, the $BaFeO_4$ cath-

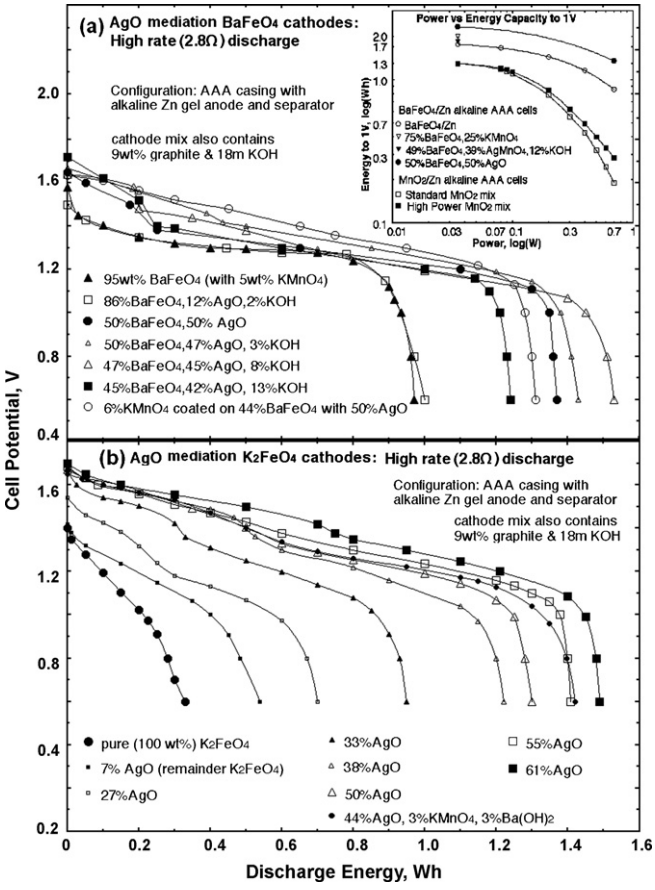

Fig. 13. Cell potential and energy capacity of alkaline cells with (a) $BaFeO_4$, (b) K_2FeO_4 cathode composites containing various weight fractions of AgO during discharge at a high constant load rate of 2.8 Ω. Cells use an alkaline AAA configuration including in the cathode 9 wt% graphite and 18 M KOH electrolyte. Inset of (a) energy at various powers during discharge of these and comparative cells [20].

ode without AgO discharges for ∼80 to 90 min and generates 0.9 Wh. The $BaFeO_4$/AgO composite cathode exhibits a maximum discharge energy higher than either component alone. The discharge capacity is ∼5-fold higher than the equivalent constant power discharge of the conventional alkaline MnO_2 cell, or ∼3-fold higher than a constant resistive load discharge [20].

5.3. Constant power comparison of MnO_2, $BaFeO_4$, and AgO/K_2FeO_4 cathodes

The unusually high specific energy/specific power of various Fe(VI) alkaline batteries is summarized in the inset of Fig. 13a. Of relevance to both practical electronics and as a fundamental energy comparison, a constant power density, rather than constant load or constant current density, offers a more stringent comparison of cathode capabilities. In this discharge the lower average cathode potential of the MnO_2 cathode (Eq. (7)) compared to Fe(VI) (Eq. (2)) must be compensated by a higher average current density which will further impair the MnO_2 charge transfer. As in Fig. 1, under conditions of constant, rapid 0.7 W discharge in an AAA cell configuration, the MnO_2 discharges to a maximum of 0.52 h (0.36 Wh), whereas a 5% $KMnO_4$/95% $BaFeO_4$ cathode (containing (4.0 g $BaFeO_4$) discharges for 1.26 h to 0.88 Wh [12]). Under the same conditions, for the composite AgO/K_2FeO_4 cathodes, a 8 wt% (0.3 g) AgO/92 wt% K_2FeO_4 cell discharges for 1.28 h to 0.90 Wh, a 20 wt% (0.7 g) AgO/80 wt% K_2FeO_4 cell discharges for 1.58 h to 1.11 Wh, and a 39 wt% (1.5 g) AgO/61 wt% K_2FeO_4 cell discharges for 2.13 h to 1.49 Wh [20].

5.4. Stabilization of K_2FeO_4 cathode with zirconia coating

As presented in the previous sections, K_2FeO_4 exhibits higher solid state stability (<0.1% decomposition per year) and higher intrinsic $3e^-$ capacity than pure $BaFeO_4$, but the rate of charge transfer is higher in the latter. Charge transfer is effectively enhanced manifold in K_2FeO_4 by small additions of AgO, while the AgO/K_2FeO_4 composite cathode exhibits higher capacity than pure $BaFeO_4$ and MnO_2 cathodes. However, the Fe(VI) forms a ferric overlayer, upon storage the bulk Fe(VI) remains active, but the overlayer passivates the alkaline cathode towards further discharge.

Due to its extreme stability over a wide temperature and environmental range, zirconia has been used as a protective coating for a variety of materials [41,42]. It has been explored to a lesser extent to protect in aqueous alkaline media, as typical zirconia deposition methods such as spray pyrolysis, plasma deposition, and colloidal deposition tend to deactivate or only partially cover electroactive surfaces [41–43]. However, in aqueous alkaline media, zirconia is practically insoluble ($K_{sp} = 8 \times 10^{-52}$) and stable [44]. Licht's group developed a novel zirconia coating, derived from an organic soluble zirconium salt. The coating method and the formation/protection mechanism for zirconia coated alkaline cathodes are detailed in Ref. [31].

The passivation of K_2FeO_4 cathode is seen in Fig. 14, in which the fresh pure K_2FeO_4 discharges well, but requires a large fraction (25 wt%) of graphite as a supporting conductive matrix, while the capacity decreases by an order of magnitude after 7 days of storage. A 1% zirconia coating dramatically improves the capacity after storage, which is further improved with a 5% KOH additive. A low level AgO additive to the cath-

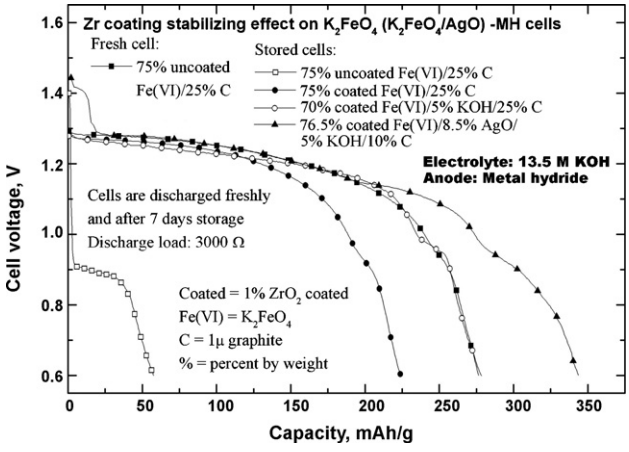

Fig. 14. Discharge capacity of K_2FeO_4 (uncoated or coated, and K_2FeO_4 composite) –MH button cells fresh and after 7 days storage [31].

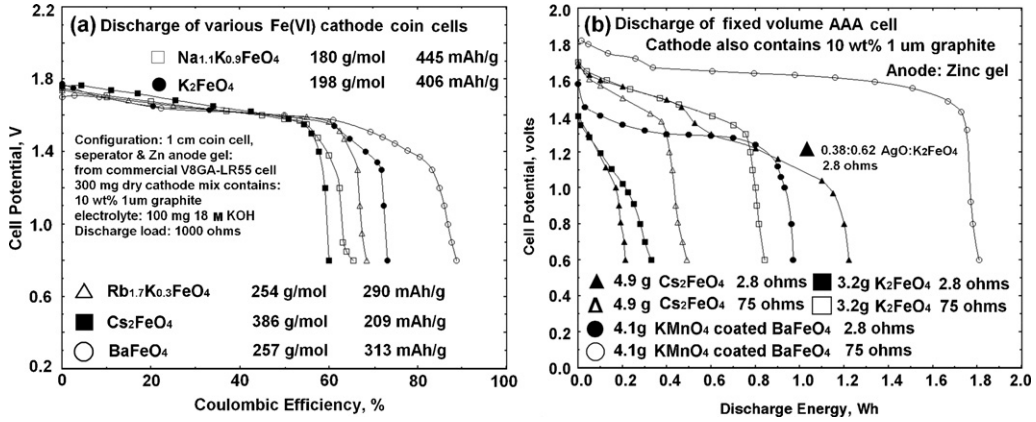

Fig. 15. (a) Alkaline super-iron coin cells (zinc anode) containing either a $BaFeO_4$, Cs_2FeO_4, K_2FeO_4, $Rb_{1.7}K_{0.3}FeO_4$, or $Na_{1.1}K_{0.9}FeO_4$ cathode discharged at a constant load of 3000 Ω. (b) Load and Fe(VI) salt effects on the discharge storage energy of alkaline K, Cs or Ba super-iron AAA cells, and compared to a K_2FeO_4/AgO [25].

ode, not only facilitates charge transfer, sustaining an effective discharge with a smaller conducting support (10%, rather than 25% graphite), but as seen in the figure yields an even greater discharge capacity than the uncoated, fresh K_2FeO_4.

6. Cathodic charge transfer of $Na(K)FeO_4$, $Rb(K)FeO_4$, Cs_2FeO_4, $SrFeO_4$ and Ag_2FeO_4 super-iron batteries

On the basis of K_2FeO_4 and $BaFeO_4$, a class of other super-iron salts include alkali Fe(VI) salts $Na(K)FeO_4$, $Rb(K)FeO_4$, Cs_2FeO_4, alkali earth Fe(VI) salt $SrFeO_4$ and a transition metal Fe(VI) salt Ag_2FeO_4 have been successfully synthesized [26]. This section focuses the cathodic charge transfer of these Fe(VI) salts in alkaline battery systems.

Fig. 15a compares the constant load discharge of super-iron batteries containing the Na, K, Rb, Cs and Ba super-iron cathodes discharged at the same condition [25]. As observed in the figure, the alternate Cs, Rb and Na mix cathodes discharge to a significant fraction of their respective intrinsic capacities of 209 mAh g^{-1} for Cs_2FeO_4, 290 mAh g^{-1} for $Rb_{1.7}K_{0.3}FeO_4$, and 445 mAh g^{-1} for $Na_{1.1}K_{0.9}FeO_4$. Each of the Fe(VI) cathodes is similar in discharge potential, but does not generate quite as a high coulombic efficiency as the $BaFeO_4$ cathode [25].

Fig. 15b compares the discharge of various pure (K_2FeO_4, Cs_2FeO_4, and $BaFeO_4$), not mixed ($Na_{1.1}K_{0.9}FeO_4$ or $Rb_{1.7}K_{0.3}FeO_4$) alkaline Fe(VI) cathodes in a configuration utilizing as a constraint a fixed volume of cathode, as compared to the configuration which utilized a fixed mass (300 mg) of cathode. The fixed cathode volume constraint of this cylindrical AAA cell configuration favors a higher mass packing of the cesium (4.9 g Cs_2FeO_4) and barium (4.4 g $BaFeO_4$) compared to potassium (3.2 g K_2FeO_4), which is due to the lower density of the latter. However, this can be compensated for by the substantially higher intrinsic 406 mAh g^{-1} capacity for the three electron Fe(VI) reduction of the potassium compared to the cesium salt or barium salts. As seen in Fig. 15b, the barium Fe(VI) cathode alkaline cell generates both at high and low load, a substantially higher discharge energy than the equivalent cesium cathode cell. This is also the case for the potassium, compared to the barium, discharge in the figure. However, as included in the figure, silver activation of the potassium salt can lead to higher discharge capacities for a K_2FeO_4/AgO composite cathode, compared to the $BaFeO_4$ cathode cell [25].

Fig. 16a compares the $SrFeO_4$, K_2FeO_4 and $BaFeO_4$ super-iron batteries under the same constant load discharge condition. Under these conditions, the strontium Fe(VI) cathode discharges

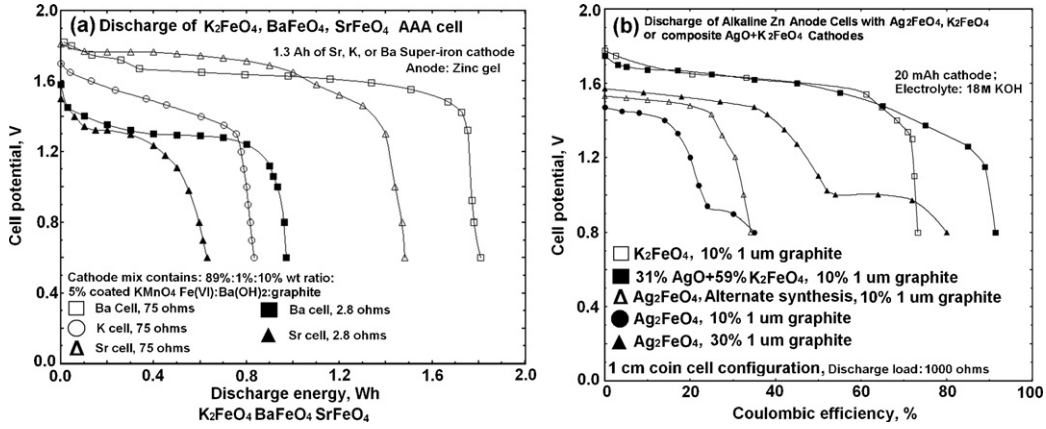

Fig. 16. (a) Alkaline super-iron AAA cells containing either a K_2FeO_4, $BaFeO_4$, or $SrFeO_4$ discharged at a constant load of 75 Ω. (b) Alkaline Zn anode super-iron cells containing either Ag_2FeO_4, AgO/K_2FeO_4 composite, or only K_2FeO_4 as a cathode, discharged at a constant load of 1000 Ω [13,26].

to ∼1.5 Wh, a significantly higher energy than generated by the K_2FeO_4 cathode, and approaches that of the $BaFeO_4$ cathode cell. The strontium cathode cells typically exhibit ∼20 to 40 mV higher open circuit voltage than the equivalent barium cell, and as seen in the figure, a higher potential average is exhibited when the strontium cell is discharged under a low (75 Ω) load. Also of significance in Fig. 16a, is the discharge of the cell under conditions of high power (small load). At a constant 2.8 Ω, the strontium cell discharges to 0.6 Wh. In addition (not shown here), a range of Fe(VI) salts were synthesized with a variety of strontium to barium ratios ($Sr_xBa_{(1-x)}FeO_4$; $x = 0.05$ to 0.95) and it is of interest that in the high power (2.8 Ω) domain, the cell discharges to ∼0.9 Wh at high potential with this discharge potential being indistinguishable from that observed in the pure barium cathode when either a $Sr_{0.25}Ba_{0.75}FeO_4$ or $Sr_{0.05}Ba_{0.95}FeO_4$ was utilized [13].

Ag_2FeO_4-Zn super-iron battery has an observed open circuit voltage of 1.86(±0.04) V. The potential under load is significantly lower (Fig. 16b), due to Fe(III) polarization losses. As seen in Fig. 16b, for the Ag_2FeO_4 and 10 wt% graphite discharge curve, the measured coulombic efficiency of the Ag_2FeO_4 salt is substantially less than that observed under the same conditions for either the K_2FeO_4 or AgO/K_2FeO_4 composite cathodes. As previously discussed for other Fe(VI) salts, these losses appear to be related to an Fe(III) blocking layer near the cathode/conductor interface. Specially, for Ag_2FeO_4, these losses are expected to be particularly acute due the relatively large, 13% ferric oxide/hydroxide impurity present as an artifact of the Ag_2FeO_4 synthesis [26]. This will intersperse insulating Fe(III) sites throughout the cathode, and inhibit charge transfer. This inhibition can be minimized by improving the conducting collector, which is in contact with the cathode salt. Hence, improvement of the cathode conductive matrix is effectuated by incorporating 30% rather than 10% graphite in the Ag_2FeO_4 salt cathode mix, resulting in an observed substantial increase in coulombic efficiency in Fig. 16b; accessing more than 80% of the theoretical $5e^-$ capacity of the Ag_2FeO_4. A two-step potential is evident during the discharge process. Consistent with the expectation that three of the five electrons are accessed in the process of Fe(VI) reduction, approximately 60% of the discharge occurs at observed higher potential. Consistent with two of the five electrons accessed in the process of Ag(I) reduction, approximately 40% of the discharge is observed to occur in a second step at a lower potential. To improve Ag_2FeO_4 charge transfer, a variety of alternative syntheses to decrease the observed 13% Fe(III) impurity in Ag_2FeO_4 salt were conducted [26]. These syntheses included variation of $Ag(NO_3)_3$ concentrations, drying temperature, and filtration conditions. Another alternative synthesis included drying under O_2, rather than vacuum, to attempt to minimize wet salt decomposition losses. It is this latter synthesized salt whose cathode product is included as the "alternate synthesis" discharge in Fig. 16b [26].

7. Summaries

Fe(VI) species have been known for over a century. Licht's group recently introduced a novel battery type based on a class of cathodes incorporating Fe(VI), sustaining facile, energetic, cathodic charge transfer. Due to their highly oxidized iron basis, multiple electron transfer, and high intrinsic energy, it has been defined Fe(VI) compounds as 'super-iron's and the new electrochemical storage cells containing them as 'super-iron' batteries.

Fe(VI) salts are capable of efficient three-electron reduction and sustains higher electrochemical storage capacity than conventional cathode materials. Discharge products of Fe(VI) are environmental benign. So far, a series of Fe(VI) compounds which have been synthesized and explored in super-iron batteries, include the synthesized Fe(VI) salts with three-electron cathodic charge capacity Na_2FeO_4, K_2FeO_4, Rb_2FeO_4, Cs_2FeO_4 (alkali Fe(VI) salts), as well as alkali earth Fe(VI) salts $BaFeO_4$, $SrFeO_4$, and also a transition Fe(VI) salt Ag_2FeO_4 which exhibits a five-electron cathodic charge storage.

Fe(VI) salts exhibit low solubility or insolubility in high concentrated alkaline electrolyte. Primary alkaline super-iron battery chemistry was established with Fe(VI) cathodes and zinc anode, and sustain higher capacity than conventional alkaline batteries. Configuration optimization, enhancement and mediation of Fe(VI) cathode charge transfer of primary Fe(VI) alkaline batteries have been investigated in detail. Small particle (1 μm) graphite and compressed carbon black have been proved as the best conductive matrix for the super-iron cathodes. Fluorinated polymer graphites provide an unusual additive to Fe(VI) cathode and are observed to simultaneously maintain two roles in the cathode; not only acting as a conductive matrix, but also adding intrinsic capacity to the cathode. Several inorganic additives (such as $SrTiO_3$) can also improve the faradaic efficiency of Fe(VI) reduction. The Fe(VI) battery potential can be shifted and controlled by the solid phase modifiers MnO_2 (decreasing ∼200 mV) and Co_2O_3 (increasing ∼150 mV). High capacity Fe(VI) salts (such as K_2FeO_4) are tend to be passivated in alkaline media and hence the charge transfer is inhibited. Two effective mediations and a coating were demonstrated. Chemical mediation of Fe(VI) with Mn(VII) or Mn(VI) improved cathodic discharge efficiency of K_2FeO_4. Chemical/electronic Ag(II) mediation of Fe(VI) redox chemistry significantly improves alkaline Fe(VI) cathodic charge transfer. Composite Fe(VI)/Mn(VI or VII), Fe(VI)/MnO_2, as well as Fe(VI)/Ag(II) cathodes provide much higher power energy capacity than the single cathodes. A novel zirconia coating derived from an organic soluble zirconium salt ($ZrCl_4$) through an organic media significantly stabilized Fe(VI) cathodes and extended the storage life of super-iron batteries.

References

[1] J.W. Mellor, A Comprehensive Treatise on Inorganic and Theoretical Chemistry, vol. XIII, Longmans, Green and Co., London, 1934, 930 pp.
[2] J. BeMiller, G. Kumari, S. Darling, Tetrahedron Lett. 40 (1972) 41.
[3] T. Schink, T.D. Waite, Water Res. 14 (1980) 1705.
[4] Y. Sakurai, H. Arai, S. Okada, J. Yamaki, J. Power Sources 68 (1997) 711.
[5] S. Hua, G. Cao, Y. Cui, J. Power Sources 76 (1998) 112.
[6] S. Licht, B. Wang, S. Ghosh, Science 285 (1999) 1039.
[7] S. Licht, B. Wang, S. Ghosh, J. Li, V. Naschitz, Electrochem. Commun. 1 (1999) 522.

[8] S. Licht, B. Wang, G. Xu, J. Li, V. Naschitz, Electrochem. Commun. 1 (1999) 527.
[9] S. Licht, B. Wang, Electrochem. Solid-State Lett. 3 (2000) 209.
[10] S. Licht, B. Wang, J. Li, S. Ghosh, R. Tel-Vered, Electrochem. Commun. 2 (2000) 535.
[11] S. Licht, V. Naschitz, S. Ghosh, B. Liu, N. Halperine, L. Halperin, D. Rozen, J. Power Sources 99 (2001) 7.
[12] S. Licht, V. Naschitz, L. Lin, J. Chen, S. Ghosh, B. Liu, J. Power Sources 101 (2001) 167.
[13] S. Licht, V. Naschitz, S. Ghosh, L. Lin, B. Liu, Electrochem. Commun. 3 (2001) 340.
[14] S. Licht, S. Ghosh, V. Naschitz, N. Halperin, L. Halperin, J. Phys. Chem. B 105 (2001) 11933.
[15] S. Licht, S. Ghosh, Q. Dong, J. Electrochem. Soc. 148 (2001) A1072.
[16] S. Licht, V. Naschitz, S. Ghosh, Electrochem. Solid-State Lett. 4 (2001) A209.
[17] S. Licht, R. Tel-Vered, L. Halperin, Electrochem. Commun. 4 (2002) 933.
[18] S. Licht, V. Naschitz, B. Wang, J. Power Sources 109 (2002) 67.
[19] S. Licht, S. Ghosh, J. Power Sources 109/2 (2002) 465.
[20] S. Licht, V. Naschitz, S. Ghosh, J. Phys. Chem. B 106 (2002) 5947.
[21] R. Tel-Vered, D. Rozen, S. Licht, J. Electrochem. Soc. 150 (2003) A1671.
[22] S. Ghosh, W. Wen, R.C. Urian, C. Heath, V. Srinivasamurthi, W. Reiff, S. Mukerjee, V. Naschitz, S. Licht, Electrochem. Solid-State Lett. 6 (2003) A260.
[23] S. Licht, R. Tel-Vered, L. Halperin, J. Electrochem. Soc. 151 (2004) A31.
[24] S. Licht, R. Tel-Vered, Chem. Commun. (2004) 628.
[25] S. Licht, V. Naschitz, D. Rozen, N. Halperin, J. Electrochem. Soc. 151 (2004) A1147.
[26] S. Licht, L. Yang, B. Wang, Electrochem. Commun. 7 (2005) 931.
[27] S. Licht, X. Yu, Environ. Sci. Technol. 39 (2005) 8071.
[28] I. Nowik, R.H. Herber, M. Koltypin, D. Aurbach, S. Licht, J. Phys. Chem. Solids 66 (2005) 1307.
[29] M. Koltypin, S. Licht, R. Tel-Vered, V. Naschitz, D. Aurbach, J. Power Sources 146 (2005) 723.
[30] S. Licht, C. DeAlwis, J. Phys. Chem. B 110 (2006) 12394.
[31] S. Licht, X. Yu, D. Zheng, Chem. Commun. (2006) 4341.
[32] M. Koltypin, S. Licht, I. Nowik, E. levi, Y. Gofer, D. Aurbach, J. Electrochem. Soc. 153 (2006) A32.
[33] W. Yang, J. Wang, T. Pan, J. Xu, J. Zhang, C. Cao, Electrochem. Commun. 4 (2002) 710.
[34] K. Bouzek, M. Schmidt, A. Wragg, Electrochem. Commun. 1 (1999) 370.
[35] J. Lee, D. Tryk, A. Fujishima, S. Park, Chem. Commun. 5 (2002) 486.
[36] M. De Koninck, T. Brousse, D. Belanger, Electrochim. Acta 48 (2003) 1425.
[37] J.C. Nardi, W.M. Swierbut, US Patent 5,895,734 (1999).
[38] H. Gohr, Electochim. Acta 11 (1966) 827.
[39] L.F. Mehne, B.B. Wayland, J. Inorg. Nucl. Chem. 37 (1975) 1371.
[40] US Federal Register; 1997; vol. 62, 367 pp.
[41] H.P. Martinz, B. Nigg, J. Matej, M. Sulik, H. Larcher, A. Hoffmann, Int. J. Refract. Met. Hard Mater. 24 (2006) 283.
[42] R. Ibanez, F. Martin, J.R. Ramos-Barrado, D. Leinen, Surf. Coat. Technol. 200 (2006) 6368.
[43] M.M. Thackeray, C.S. Johnson, J.-S. Kim, K.C. Lauzze, J.T. Vaughey, N. Dietz, D. Abraham, S.A. Hackney, W. Zeltner, M.A. Anderson, Electrochem. Commun. 5 (2003) 752.
[44] W.F. Linke, Solubilities of Inorganic and Metal-Organic Compounds, 4th ed., Van Nostrand, Princeton, NJ, 1958, 1695 pp.